American Mineralogist, Volume 83, pages 1083–1091, 1998

Thermal annealing of radiation damaged titanite

J. CHROSCH,[1] M. COLOMBO,[1] T. MALCHEREK,[1] E.K.H. SALJE,[1,*] L.A. GROAT,[2] AND U. BISMAYER[3]

[1]Department of Earth Sciences, University of Cambridge, Downing Street, Cambridge CB2 3EQ, U.K.
[2]Department of Earth and Ocean Sciences, University of British Columbia, 6339 Stores Road, Vancouver V6T 1Z4, British Columbia, Canada
[3]Mineralogisch-Petrographisches Institut, Universität Hamburg, Grindelallee 48, D-20146 Hamburg, Germany

ABSTRACT

Radiogenic impurities of 400 to 800 ppm U and Th in titanite, $CaTiSiO_5$, lead to moderate radiation damage ($\approx 1.5 \times 10^{18}$ α-decay events/g) and therefore to partial amorphization (≈30%). Powder X-ray diffraction on such damaged titanite from the Cardiff locality in Canada shows that two modifications of the crystalline material coexist. Both modifications are structurally β phase but differ systematically in their lattice parameters and also in their chemical composition. One modification exhibits strong particle size broadening in X-ray diffraction patterns, whereas it is almost unstrained with respect to fully annealed titanite. The other modification shows large strain broadening and increased specific volume (about 3%) due to a high concentration of defects. The unstrained modification consists of small nucleation centers in the damaged material, and it grows when the sample is annealed. At annealing temperatures above 823 K, this modification dominates rapidly and replaces the strained titanite. The results of Rietveld refinement of the annealed samples and of the time evolution of isothermal annealing studies are discussed. The analysis of volume strain and of structural strain resulting from the peak profiles suggests a temperature-dependent activation energy for the recrystallization process, with $E_A \approx 380$ kJ/mol at $T > 873$ K and $E_A \approx 500$ kJ/mol at temperatures 773 K $< T <$ 873 K.

INTRODUCTION

Titanite, $CaTiSiO_5$, is an accessory mineral in a wide variety of igneous and metamorphic rocks. The structure consists of chains of corner-sharing TiO_6-octahedra parallel to the *a* axis, cross-linked by edge-sharing chains of CaO_7 polyhedra parallel to [101]. Isolated SiO_4 tetrahedra share corners with both structural units (Speer and Gibbs 1976; Taylor and Brown 1976). In the room-temperature α phase ($P2_1/a$), the Ti atoms are located in off-center positions within the TiO_6 octahedra. The orientation of the off-center dipole vectors are nearly parallel within an individual TiO_6 chain but in opposite directions between neighboring chains.

Synthetic and natural titanites undergo a phase transition between the α phase and the β phase at 496 K. This phase transition has been thoroughly investigated (Speer and Gibbs 1976; Taylor and Brown 1976; Higgins and Ribbe 1976; Oberti et al. 1991; Bismayer et al. 1992; Salje et al. 1993a; Zhang et al. 1995; Chrosch et al. 1997), and it is mainly related to a change in the position of the Ti atoms within the octahedron. The average symmetry of the β phase is described by the space group $A2/a$ ($C2/c$). Careful investigation of optical birefringence, IR and Raman spectra, dielectric response, heat capacity, and X-ray diffraction analysis indicate that the observed $A2/a$ symmetry above 496 K results from a loss of long-range coherence between individual Ti off-center dipoles (Zhang et al. 1995; Bismayer et al. 1992). Salje et al. (1993a), Chrosch et al. (1997), and Zhang et al. (1997) showed that a further phase transition, $\beta \leftrightarrow \gamma$, occurs at 825 K.

The β phase is observed at room temperature for samples with Ti partly substituted by Al or Fe (Higgins and Ribbe 1976; Oberti et al. 1991). The structural formula of titanite may be written symbolically as $CaTi(SiO_4)O$, with substitution possible at both cation and anion sites within the structure. Substitution of Ti^{4+} by lesser charged cations is charge balanced with $(OH)^-$ or F^- replacing O^{2-}. The Ca position is sevenfold coordinated and can accommodate minor amounts of Na, REEs, Y, U, and Th (Hughes et al. 1997). As a result of the two latter radiogenic substitutions, titanites may suffer substantial radiation damage (Hawthorne et al. 1991; Vance and Metson 1985). The extent of this damage depends on the radiation dose (Ewing 1987; Ewing et al. 1987) due to the progressive overlap of α-recoil collision cascades. Naturally occurring titanite has been found either as an essentially crystalline phase or as a mixture of amorphous and crystalline regions (Hawthorne et al. 1991; Vance and Metson 1985).

* E-mail: es10002@esc.cam.ac.uk

0003–004X/98/0910–1083$05.00

We were motivated to investigate the damage annealing of titanite for two reasons. First, titanite shows both structural damage by radiation and also structural phase transitions. This coincidence makes titanite an ideal model compound for the systematic investigation of the interplay between radiation damage and subtle structural transformations. Second, the storage of nuclear waste may involve the radiation damage of titanite-type materials. In fact, the Canadian Nuclear Fuel Waste Management program has considered the possibility of waste storage with glass ceramics containing crystalline titanite embedded in an aluminosilicate glass (Hayward and Cecchetto 1981; Hayward 1988; Vance and Metson 1985; Hawthorne et al. 1991). For such applications it is essential to understand the role played by the radiation damage on the structural stability of the host material.

Experimental procedures

The titanite used is from the Cardiff locality in Ontario, Canada. The material was previously described by Hawthorne et al. (1991) as sample M28696. According to Fleet and Henderson (1985), Vance and Metson (1985), Hawthorne et al. (1991), and Lumpkin et al. (1991), Cardiff titanite contains substantial amounts of Al_2O_3 and Fe_2O_3, replacing Ti on the octahedral sites. The Al_2O_3 content varies from 3.4 to 6.4 wt%, with Fe_2O_3 varying from 3.6 to 0.5 wt%, respectively. Therefore, on average, at least 20% of the octahedral sites are occupied by Fe and Al, rather than Ti. The U and Th concentrations reported for these samples are equally variable (between 400 and 800 ppm). Based on an equivalent uranium (EU) content of 500 ppm and an estimated age of 1000 Ma, Vance and Metson (1985) conclude a dose of 1.5×10^{18} α-decay events/g, corresponding to about 30% of the dose needed to render the structure completely X-ray amorphous.

The starting material used in this study was a dark red color, with well-developed crystal faces and a glassy appearance. Some impurities and alteration products could be identified by X-ray diffraction, with an estimate of the volume fraction provided by Rietveld refinement. The principal impurity phases are fluorite ($\approx$8 vol%) and calcite ($\approx$1 vol%). Other possible phases, which also crystallize in the fluorite structure, include thorianite, ThO_2, and uraninite, UO_{2+x}. Due to the presence of heavy elements, these phases might contribute to the X-ray scattering background, even though their actual volume fraction is well below 1%. Weak magnetism of parts of the titanite also suggests the presence of ilmenite or magnetite. Up to 28 vol% of quartz were detected in few of the annealed and quenched sample batches. As there is no evidence of any temperature or time dependence dominating the appearance of this phase, it is likely that quartz was initially present as an alteration product in parts of the titanite crystal, also because the majority of quenched sample batches contained no quartz detectable by X-ray diffraction.

In-situ high temperature X-ray powder diffraction

Part of the sample was crushed and milled to a fine-grained powder for annealing inside a high-temperature diffractometer. Si was added to the powder as internal standard for X-ray powder diffraction analysis using monochromatic ($CuK\alpha_1$) radiation in the Bragg-Brentano geometry. The diffracted intensities were measured with a 120° curved PSD detector (INEL) between $2\theta_{min} = 3°$ and $2\theta_{max} = 120°$. The high-temperature diffractometer was previously described by Salje et al. (1993b). Isothermal annealing experiments were performed within the heating stage of the diffractometer at 573, 823, and 973 K under vacuum, using the same powder sample in all. The annealing times extended to 69.5, 27.5, and 44 h. The first four diffraction patterns at each temperature were counted for 15 min. The subsequent patterns were collected for 2 h each.

Guinier powder diffraction on quenched samples and Rietveld refinement

Small amounts ($\approx$35 mg) of the initial titanite crystal were wrapped in platinum foil and annealed at temperatures between 473 and 1123 K. At temperatures above 700 K, samples were kept under a nitrogen atmosphere during annealing. The average weight loss was between 0.08% at 473 K and 0.7% at 1123 K. Following Hawthorne et al. (1991) this weight loss can be attributed to the combined presence of large F concentrations and H_2O in Cardiff titanite. The principal evolving gas species under these conditions is H_2 for samples with F (but H_2O for samples lacking F) at moderate temperatures, whereas at higher temperatures, $T \geq 1073$ K, a mixture of SiF_4, O_2, F, HF, and H_2 escapes.

The quenched titanite samples were crushed in an agate mortar and ground to a fine powder using a Spex Micro-Ballmill. The sample material was mixed with Si powder, used as a standard for calibration of diffraction angles. The mixture was dispersed onto mylar foil, using amylacetate as an adhesive. X-ray diffraction patterns were recorded using a Huber G600 Guinier step scan diffractometer, with sample spinner and monochromatic $CuK\alpha_1$ radiation. Diffraction patterns were recorded in the range $6° \leq 2\theta \leq 90°$ with stepsize 0.02°. Intensity at each point was counted for 40 s.

Rietveld refinement was performed using the GSAS software package (Larson and Von Dreele 1994). A pseudo-Voigt profile function corrected for peak asymmetry due to axial divergence (Finger et al. 1994) was employed. Calibration of the asymmetry parameters using quartz and silicon yielded values of S/L = 0.049 and H/L = 0.032, where 2S is the effective height of the sample, 2H is the effective length of the detector slit and L is the average distance between the sample and the detector.

Background intensity contribution from the mylar foil of the sample holder was subtracted from the patterns before refinement. Under the given conditions (small grain size, Guinier geometry) the obtained profile func-

TABLE 1. Structural parameters of heated Cardiff titanite (1123 K, 3 d)

Type	x	y	z	Occ.	U*100
Ca	0.25	0.1669(8)	0	1	3.3(4)
Ti	0.5	0	0.5	0.74(4)	2.1(3)
Al	—	—	—	0.26(4)	—
Si	0.75	0.181(1)	0	1	1.8(4)
O(1)	0.75	0.066(2)	0.5	1	2.5(6)
O(2)	0.909(2)	0.062(1)	0.193(2)	1	1.9(5)
O(3)	0.367(2)	0.291(1)	0.350(2)	1	1.8(4)

Note: Space group = *A2/a*. The lattice parameters are reported in Table 2. R_p = 0.0944, R_{wp} = 0.1372.

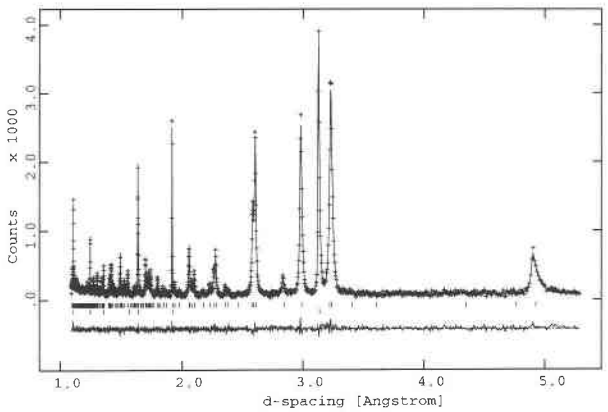

FIGURE 1. Observed and calculated diffraction pattern for Cardiff titanite annealed at 1123 K for 3 d. The lower row of peak position markers indicates the Si standard, the upper row indicates titanite. The difference between observed and calculated intensity is shown below these markers.

tions are entirely Lorentzian. Therefore, only two profile parameters had to be refined for each phase. Preferred orientation of titanite parallel to the {110} cleavage planes was refined using the March-Dollase formalism. Scattering functions for uncharged atoms were used.

ROOM-TEMPERATURE POWDER DIFFRACTION

Recrystallized titanite

A full structure refinement was performed on the sample annealed for 3 d at 1123 K, which prior TEM observations showed to be fully recrystallized. The results are shown in Table 1 and the diffraction pattern is shown in Figure 1. The refined occupancy of Al replacing Ti on the octahedral position is 26 ± 4 mol% ≈6.8 wt% Al_2O_3, which is in good agreement with the analysis given by Vance and Metson (1985) and in Table 14 of Hawthorne et al. (1991). The refined set of parameters was used in all subsequent refinements of progressively metamict samples, including untreated material. The atomic positions and isotropic temperature factors were held fixed, whereas the Ti/Al ratio on the octahedral positions was refined. Single-crystal structure refinements of metamict Cardiff titanites (Hawthorne et al. 1991) show only minor deviations of the average structure from the structure of recrystallized material. Therefore the assumption of an undisturbed average structure must be valid. However, in terms of Al content, the refinements with fixed structural parameters can only be expected to give a qualitative estimate of the true impurity concentration. Additional presence of Fe is not expected to alter the refined Al content significantly, as the scattering powers of Ti and Fe are similar.

The obtained R-values were generally large ($W_p \approx$ 10%). This is due to relatively high levels of background noise, whereas the difference curve ($I_{obs} - I_{calc}$) for heated titanite in Figure 1 only shows small deviations between the measured and refined peak profiles.

Metamict titanite

Bragg peaks in this natural Cardiff titanite are split as clearly seen at ≈2.6, 3, and 3.2 Å in Figure 2. This can be attributed to contributions from two different microstructural fractions of titanite. One fraction exhibits predominantly strain broadening, corresponding to Bragg peaks shifted toward larger d-spacings. This strained fraction will be called titanite II.

The other fraction, assigned to smaller d-spacings, has approximately the same cell parameters as the final, annealed titanite. Hence, this fraction can be regarded as almost unstrained, and we will refer to it as titanite I. Broadening of the corresponding Bragg peaks is predominantly caused by small particle size.

Rietveld refinement of natural Cardiff titanite and of partially annealed samples was completed using two distinct titanite modifications. Structurally, these two modifications were taken to be identical, apart from the variation of the Al concentration on the octahedral position and their unit-cell dimensions. Unit-cell parameters and resulting strain values are listed in Tables 2 and 3, respectively. The diffraction signals of both titanites merge rapidly at temperatures above 873 K, so that values for only one structure are reported at this temperature.

Various strain parameters can be calculated for both microstructural titanite fractions. The components of the strain tensor and a corresponding scalar strain as well as the volume strain can be obtained from the lattice parameters, using the cell parameters of heated titanite (Table 2) as reference point. An isotropic structural strain, e_p, is calculated based on the peak profile parameters (Larson and Von Dreele 1994). The structural strain of the titanite II component is plotted in Figure 3 as a function of annealing time. The observed volume strain in Cardiff titanite is approximately 3%, a value that also has been reported by Vance and Metson (1985). The logarithm of the volume strain during heating at 773, 873, and 973 K is shown in Figure 4 as function of logarithmic time.

IN-SITU X-RAY DIFFRACTION

The powder diffraction pattern of the starting material (cf. Fig. 5, top, t = 0) shows a high background diffraction signal of the amorphous matrix with superimposed

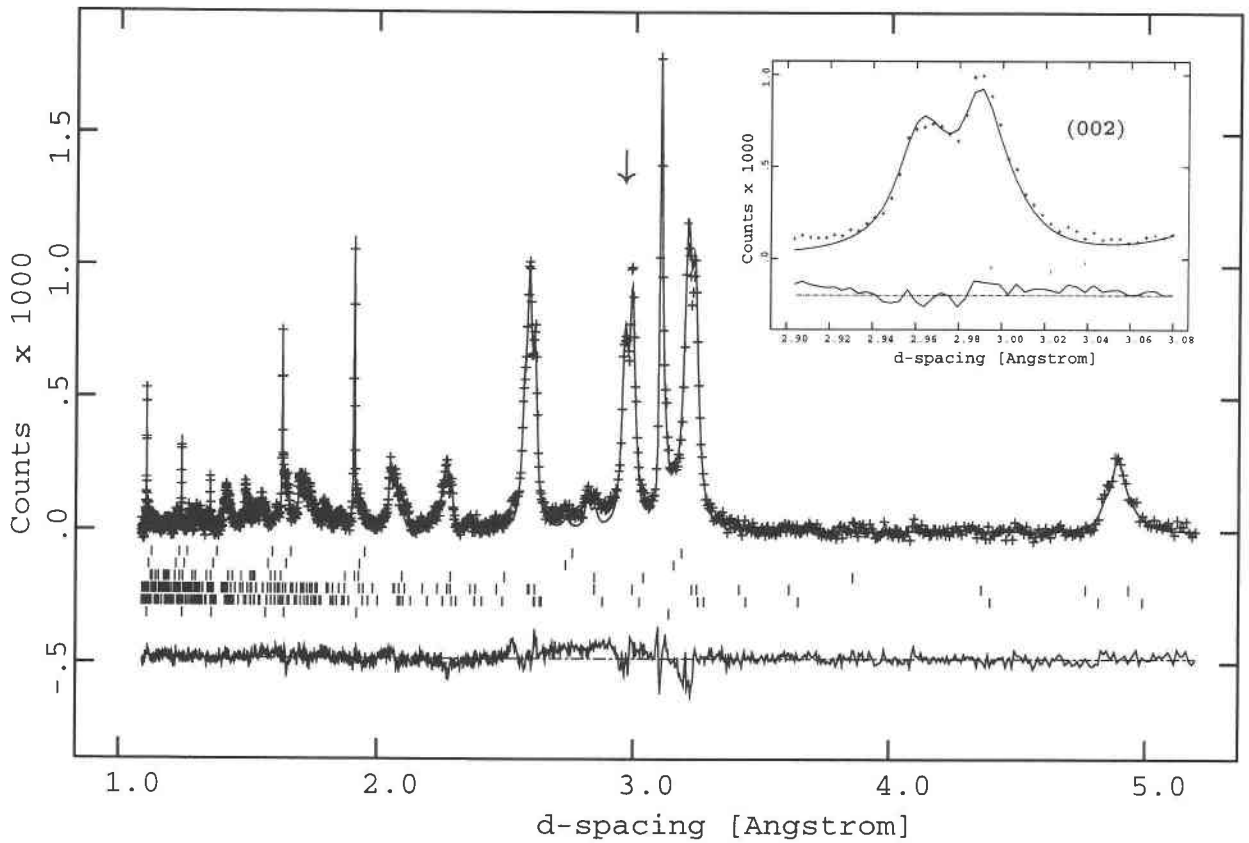

FIGURE 2. Observed and calculated diffraction pattern of untreated Cardiff titanite. Peak positions are shown for five phases (from bottom to top, approximate volume fraction in parentheses): Si-standard. titanite II (≈34%), titanite I (≈57%), calcite $CaCO_3$ (≈1%), fluorite CaF_2 (≈8%), and thorianite, ThO_2 (<1%). The difference curve of observed and calculated intensities is shown below the peak markers. The inset shows a magnified portion of the diffraction pattern (position as indicated by the arrow). The two maxima are the (002) peaks of titanite I and II, respectively.

powder diffraction lines of the crystalline parts of the sample. The Bragg peaks are only weakly broadened. The line widths are equivalent to coherent length in excess of 500 Å. As in the case of the (002)-peak (Fig. 2), the fine structure of the powder lines at $2\theta \approx 27.5°$, clearly shows two peaks ($\bar{2}11$) related to the two different modifications of titanite (the splitting can be seen in the pattern at 573 K, Fig. 5, top). Indexing of the extra peaks with symmetry forbidden indices, $k + l = 2n + 1$, indicative of the α phase, could be ruled out on grounds of the equal intensity of both peaks. Superstructure reflections due to off-centering of the Ti-cations in the α phase are generally much weaker than the fundamental reflections $k+ l = 2n$ (Taylor and Brown 1976). We assign the peak at smaller 2θ angle to titanite II and the peak at larger diffraction angle to titanite I.

Annealing the sample at 573 K leads to the time evolution of the powder spectrum shown in Figure 5, top. The intensity of the ($\bar{2}11$)-reflection increases simultaneously for both phases, titanite I and II. The quantitative increase is similar for both peaks, with no indication that significant changes of the relative intensities of any powder peak occur, i.e., the time evolution is characterized by a uniform increase of all crystalline diffraction signals. This clearly shows that the amounts of both titanites in the sample increase without major structural changes.

Further annealing at 823 K follows a very different pattern (Fig. 5, middle). The Bragg peak of titanite I swiftly gains intensity, whereas the integrated diffraction signal of titanite II decreases. However, the height of the broad titanite II peak increases with time (Fig. 6), whereas the concomitant shift toward higher diffraction angles indicates a decrease of the lattice volume (Fig. 7) for this component.

Annealing at 973 K is similar to that at 823 K. The remaining diffuse scattering signal of titanite II disappears gradually (Fig. 5, bottom) and merges with the diffraction signal of titanite I within an annealing time of approximately 30 h. The final annealing stage is now identical to the powder diffraction pattern of a standard titanite sample in its β phase (Chrosch et al. 1997).

The recrystallization is seen as the general increase of the powder peaks (Fig. 8) and a simultaneous decrease of the diffuse background diffraction, arising from the

TABLE 2. Lattice parameters of quenched Cardiff titanite

T (K)	t (h)	a (Å)	b (Å)	c (Å)	β (°)	V (Å³)
298	0	7.124(2)	8.779(2)	6.619(2)	114.10(2)	377.9(2)
		7.063(1)	8.704(2)	6.548(1)	113.93(2)	367.9(1)
673	0.1667	7.124(3)	8.778(3)	6.616(3)	114.08(4)	377.7(2)
		7.060(6)	8.735(8)	6.536(7)	114.02(9)	368.1(5)
673	0.5	7.116(3)	8.773(3)	6.607(3)	113.96(5)	377.0(3)
		7.049(5)	8.737(7)	6.523(6)	113.76(8)	367.7(6)
673	1.0	7.122(2)	8.781(2)	6.618(2)	114.09(3)	377.8(2)
		7.064(2)	8.718(3)	6.553(3)	113.96(3)	368.8(3)
773	1.0	7.112(3)	8.767(3)	6.609(3)	114.09(4)	376.2(3)
		7.059(3)	8.719(4)	6.546(3)	113.92(4)	368.3(3)
773	16.0	7.095(2)	8.746(3)	6.592(2)	114.11(3)	373.3(2)
		7.051(2)	8.701(2)	6.540(2)	113.92(2)	366.7(2)
773	336.0	7.079(1)	8.730(1)	6.579(1)	114.03(2)	371.4(1)
		7.027(4)	8.695(5)	6.523(4)	113.91(5)	364.3(4)
773	744.0	7.080(3)	8.730(4)	6.577(3)	114.02(4)	371.3(3)
		7.048(4)	8.705(5)	6.534(4)	113.89(4)	366.6(4)
873	24.0	7.0620(7)	8.715(1)	6.5602(7)	114.02(1)	368.76(7)
		7.032(2)	8.694(3)	6.536(2)	113.80(3)	365.6(2)
873	90.0	7.0598(5)	8.7067(7)	6.5554(5)	113.986(7)	368.15(5)
		7.017(3)	8.692(5)	6.515(3)	113.83(4)	363.5(3)
873	264.0	7.0580(6)	8.7070(8)	6.5542(6)	114.998(8)	367.97(6)
		7.036(3)	8.686(4)	6.533(3)	113.85(4)	365.2(3)
873	624.0	7.0544(5)	8.7022(7)	6.5485(5)	113.997(7)	367.25(5)
		7.032(2)	8.682(2)	6.533(2)	113.88(2)	364.7(2)
973	0.117	7.0472(8)	8.701(1)	6.5480(9)	114.01(1)	366.77(9)
973	0.25	7.0458(4)	8.6970(5)	6.5464(4)	113.987(5)	366.50(4)
973	0.5	7.0432(5)	8.6962(7)	6.5443(5)	113.984(8)	366.22(5)
973	1.0	7.0418(5)	8.6953(7)	6.5439(5)	113.995(7)	366.05(5)
973	48.0	7.0419(5)	8.6928(7)	6.5392(5)	113.953(7)	365.81(5)
1123	72.0	7.0469(4)	8.6901(5)	6.5372(4)	113.944(5)	365.88(3)

Note: Two sets of parameters are given in cases where the refinement of two titanite phases was possible.

amorphous regions of the sample. In order to quantify this effect the background scattering was integrated between $2\theta = 26.8°$ and $2\theta = 27.8°$ and plotted as a function of time (Fig. 9). [This 2θ range is close to the position of the diffuse halo at d = 3 Å in electron diffraction patterns of Cardiff titanite (Hawthorne et al. 1991)]. The decrease of the diffraction signal of the amorphous matrix is clearly visible. A roughly linear relationship between the decrease of the background scattering and the increase of the Bragg intensity of the $(\bar{2}11)$ peak of titanite I is shown in Figure 10. The position of the $(\bar{2}11)$ peak changes very little with annealing, and the effective particle size of the final stage of annealing is about 800 Å.

DISCUSSION

All of the above observations were made with respect to β titanite as the stable crystalline state. in radiation damaged titanite. This correlates with the tendency of substitutional defects to destabilize the α phase in favor of the β phase (Hughes et al. 1997; Oberti et al. 1991). The Cardiff sample contains substantial amounts of Fe and Al, and one might expect at least a partial suppression of the α phase, e.g., similar to titanite from the Rauris locality (Zhang et al. 1995). Annealing the sample does not seem to produce the equilibrium phase (i.e., the α phase) of titanite, but rather the high-temperature β phase. This observation might well be explained by the high degree of Al content of the sample before and after annealing.

A possible interpretation of the observed peak splitting in metamict titanite is that the strain-broadened fraction stems from a titanite structure, which is exposed to stress from the surrounding amorphous parts of the material. Moreover, high defect concentrations in these crystalline areas cause the large volume strain (≈3%) observed for this fraction. This volume strain might define a limiting value for the crystalline state above which long-range order ceases to exist. Such a limit to the defect concentration taken up by the crystalline structure also has been found in zircon (Holland and Gottfried 1955).

Titanite I can be attributed to nuclei of recrystallized titanite inside the amorphous regions or alternatively to remnants of titanite that had never been subject to radiation damage. The latter interpretation requires a very inhomogeneous distribution of U and Th in the material. The former interpretation has been suggested by Holland and Gottfried (1955), who reported a second, defect-free and misoriented zircon phase, if the parent structure had been subject to intermediate radiation dosage between 2–9 × 10^{18} α-decay events/g. These authors also suggest that the nucleation of this undamaged phase from the amorphous matrix is due to thermal spikes caused by the passage of α particles. Similar peak splitting in metamict zircon, albeit at higher diffraction angles, was also re-

TABLE 3. Strain values ($\times 10^3$)

T (K)	t (h)	ϵ_{11}	ϵ_{22}	ϵ_{33}	ϵ_{13}	e_s	e_v	e_p
298	0	9.7	10.3	12.5	−0.4	18.9	32.8	7.0
		2.4	1.6	1.6	0.2	3.3	5.5	1.6
673	0.1667	9.9	10.1	12.1	−0.3	18.6	32.4	6.3
		1.2	5.1	−0.2	0.4	5.3	6.2	7.6
673	0.5	9.7	9.5	10.7	−0.2	17.3	30.3	6.7
		1.7	5.4	−2.2	0.5	6.2	5.0	−1.6
673	1.0	9.5	10.4	12.4	−0.4	18.8	32.7	5.9
		2.4	3.2	2.4	0.0	4.7	8.0	−3.6
773	1.0	8.1	8.9	10.9	−0.4	16.3	28.2	5.8
		2.0	3.3	1.3	1.0	4.1	6.6	−4.0
773	16.0	5.4	6.4	8.3	−0.3	11.9	20.3	8.4
		0.7	1.2	0.4	0.0	1.4	2.2	−0.6
773	336.0	3.9	4.6	6.4	−0.4	8.9	15.0	6.8
		−2.6	0.6	−2.2	−0.1	3.4	−4.3	−4.5
773	744.0	4.1	4.6	6.1	−0.3	8.7	14.8	10.7
		0.6	1.7	−0.5	0.2	1.9	2.0	−5.0
873	24.0	1.5	2.8	3.5	−0.3	4.8	7.9	4.3
		−1.0	0.5	−0.3	−0.4	1.4	−0.8	−5.0
873	90.0	1.5	1.9	2.8	−0.2	3.7	6.2	3.1
		−3.3	0.2	−3.4	−0.2	4.8	−6.5	−5.0
873	264.0	1.2	1.9	2.6	−0.2	3.5	5.7	0.5
		−0.9	−0.5	−0.7	−0.2	1.3	−2.0	−0.5
873	624.0	0.7	1.4	1.7	−0.1	2.3	3.7	0.02
		−1.7	−0.9	−0.7	−0.3	2.1	−3.3	−4.6
973	0.117	−0.5	1.2	1.7	−0.4	2.2	2.4	5.5
973	0.25	−0.5	0.8	1.4	−0.3	1.8	1.7	4.3
973	0.5	−0.8	0.7	−1.1	−0.4	1.7	0.9	1.6
973	1.0	−1.1	0.6	1.0	−0.4	1.8	0.5	0.44
973	48.0	−0.8	0.3	0.3	−0.2	1.0	−0.2	0.4

Note: ϵ_{11} to ϵ_{13} = monoclinic strain tensor; e_s = scalar strain; and e_v = volume strain, based on reference lattice parameters of Cardiff titanite heated 3 d at 850 °C. The isotropic structural strain, e_p, is calculated based on the profile parameters of the Rietveld refinement.

ported by Murakami et al. (1991). According to Vance and Metson (1985) the structure of titanite is two to three times more susceptible to radiation damage than the structure of zircon. Taking this correction to the dosage into account, the diffractometer traces shown in this study, e.g., Figure 2 and Figure 5, can be directly compared with the corresponding diffractometer traces of zircon shown by Holland and Gottfried (1955), i.e., sample 4–14 in Figure 3 of their paper.

The strain analysis of annealed samples can be used to obtain insight into the activation energy of the recrystallization process. Whereas the structural strain seen in titanite II, or in the merged peaks at higher temperatures (Figure 3), appears to decay exponentially at temperatures above 873 K, it remains unchanged or it even increases slightly at lower temperatures. An exponential function $e_p(t) = e_p(t_o)\exp(-kt)$ can he fitted to the high-temperature data. Assuming that the time constant k follows a simple Arrhenius behavior,

$$k = k_o \exp\left(\frac{-E_a}{k_B T}\right) \quad (1)$$

an activation energy $E_A \approx 380$ kJ/mol can be calculated. The preexponential factor follows as $k_o \approx 2 \cdot 10^{17}$Hz, which, given a vibrational frequency in the THz region commonly found in solids, implies a large entropy of activation ($\approx 1.4\ R$).

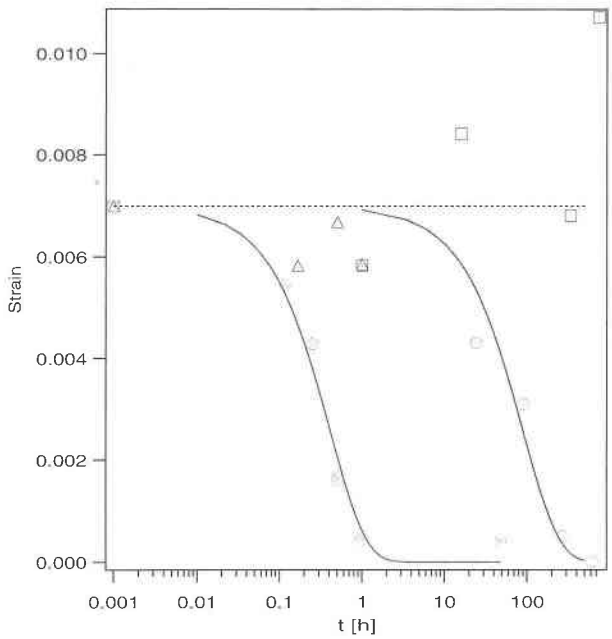

FIGURE 3. Observed isotropic structural strain e_p (titanite II) as function of time for 673 K (triangles), 773 K (squares), 873 K (open circles), and 973 K (crossed circles). The curves show calculated exponential decay functions at 873 K and 973 K.

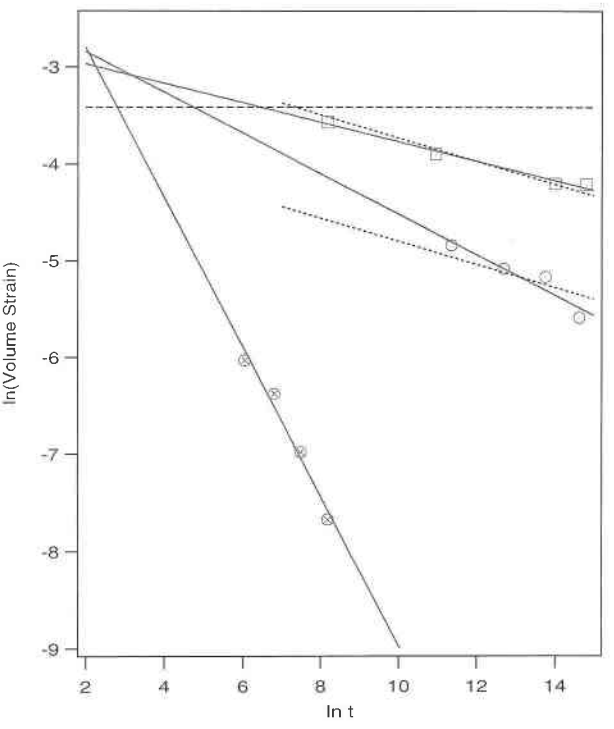

FIGURE 4. Log-Log plot of volume strain for 773 K (squares), 873 K (open circles), and 973 K (crossed circles). The horizontal line indicates the initial volume strain. The solid lines show a best fit to the data, whereas the two dashed lines represent the approximation used to derive an activation energy in the low temperature regime.

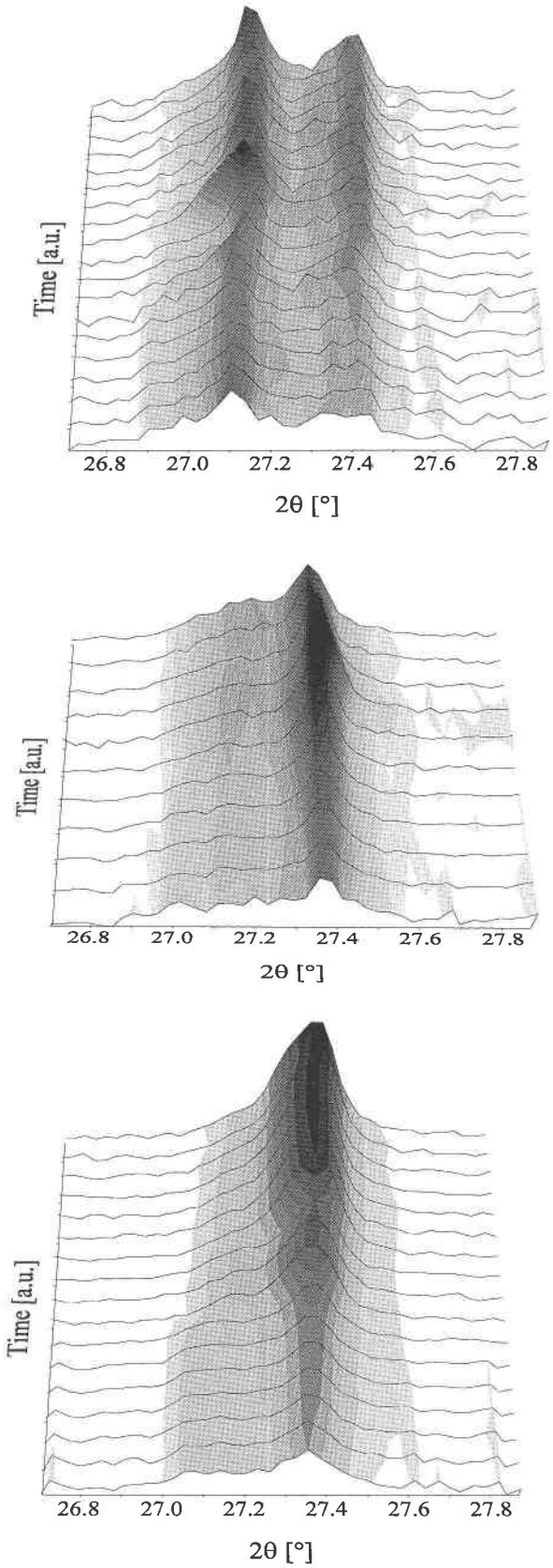

FIGURE 5. Diffraction pattern as function of time during annealing experiments at 573 K (top), 823 K (middle), and 973 K (bottom). The intensity at 973 K is plotted on a logarithmic scale. The timescale is indicated by horizontal lines at ~3 h intervals. The time axis points from bottom to top in each diagram. ←

The volume strain shows a clear time dependence even at 773 K (Fig. 4). The approximately linear correlation between $\ln(e_v)$ and $\ln(t)$ seen in Figure 4, suggests a power law behavior $e_v \propto t_n$. The different slopes indicate that the exponent n is strongly temperature dependent and no attempt was made to determine the activation energy from equal fractions of transformation over the whole temperature range. However, whereas the kinetics are clearly different for small volume strains seen at high temperatures, the behavior at lower temperatures can be approximated using a single time exponent for 773 and 873 K, as shown in Figure 4. Using this approximation an activation energy in the order of 500 kJ/mol is obtained. This value depends crucially on the value of the exponent n. Hence, provided that the power law behavior describes the kinetics correctly, the activation energy rapidly decreases with increasing temperature, i.e., with increasing n.

The kinetic behavior of the Bragg intensities at 823 K (Fig. 8) and the position of the diffuse scattering (Fig. 7) show the same characteristic time evolution, a rapid change at times shorter than 2 h and a much weaker time dependence for the later stages. Such a multistage behavior is commonly observed for other radiation damaged material (Weber 1990). The short time regime is then attributed to the annealing of Frenkel defects in weakly damaged regions whereas the late time regime is dominated by the propagation of the stable, crystalline phase into the unstable, amorphous matrix. Our results can be analyzed within the same theoretical model. The diffuse scattering is then associated with regions of high defect

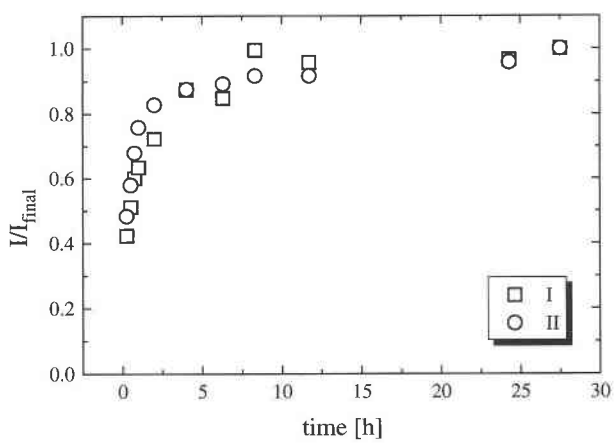

FIGURE 6. Relative intensity of the $(\bar{2}11)$-peak for titanite I and for titanite II as function of annealing time at 823 K.

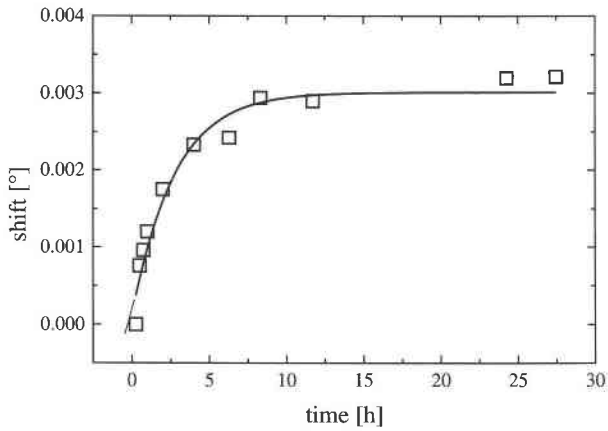

FIGURE 7. Position of the diffuse maximum, corresponding to titanite II, as a function of time at 823 K.

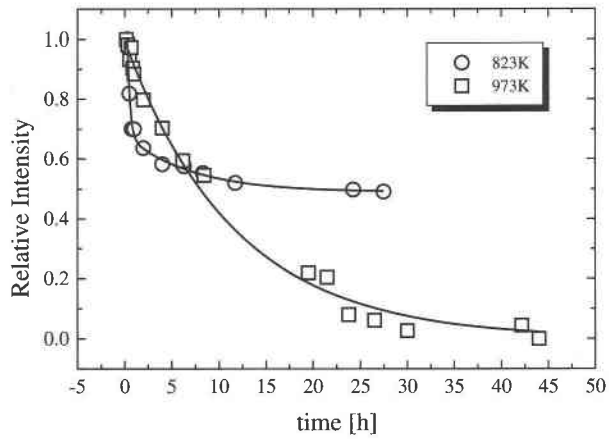

FIGURE 9. Background scattering between $2\theta = 26.8°$ and $2\theta = 27.8°$ as function of annealing time at 823 and at 973 K.

densities but remaining weak crystallinity, i.e., small grain sizes. At high temperatures this diffuse scattering is observed toward the low angle side of the Bragg peak, as the particle size of the defect rich, but crystalline material decreases. Annealing leads to a shift of the diffraction maximum that corresponds to a strain release of some 3%. The recombination of Frenkel defects usually dominates the low-temperature annealing behavior in radiation damaged zircon (Weber 1990; Vance and Metson 1985) whereas growth phenomena are most relevant at higher temperatures.

We have obtained two different activation energies using strain measurements. At the low-temperature limit (773–873 K) of the recrystallization process $E_A \approx 500$ kJ/mol is observed, whereas a more accurate estimate of $E_A \approx 380$ kJ/mol is calculated at higher temperatures (873–973 K). Seen in context with the decreasing time exponent (Fig. 4) this might indeed indicate a change in mechanism with increasing annealing temperature, i.e., a crossover from defect annealing to rapid growth of crystalline areas.

The combination of continuous radiation damage and partial recrystallization of metamict titanite can drive this material into a state of microstructural and possibly chemical inhomogeneity. We distinguish between three fractions of titanite: (1) The original titanite structure expands by 3% with respect to the undamaged material. Any part of the structure that is subjected to larger volume strains is so heavily damaged that it does not contribute to the long-range order seen by the X-ray diffraction experiments. (2) These heavily damaged areas of titanite form the amorphous matrix. The total volume fraction of amorphous material with respect to the crystalline part depends on the radiation dose, whereas the structural state of both fractions appears to be more or less constant. (3) The presence of small particles of largely undamaged titanite in the untreated material might be due to regions in the metamict crystals that are never affected by α-decay events. This can be caused either by inhomogeneous distribution of U and Th in the sample (Murakami et al. 1991) or by channeling effects of the

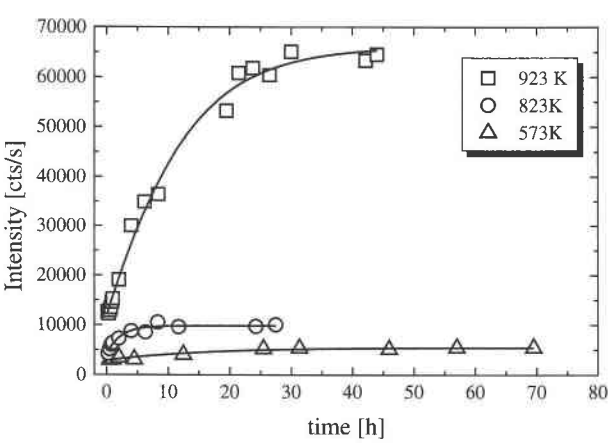

FIGURE 8. Powder diffraction intensity in $(\bar{2}11)$ (titanite I) as function of time. The curves are guides to the eye.

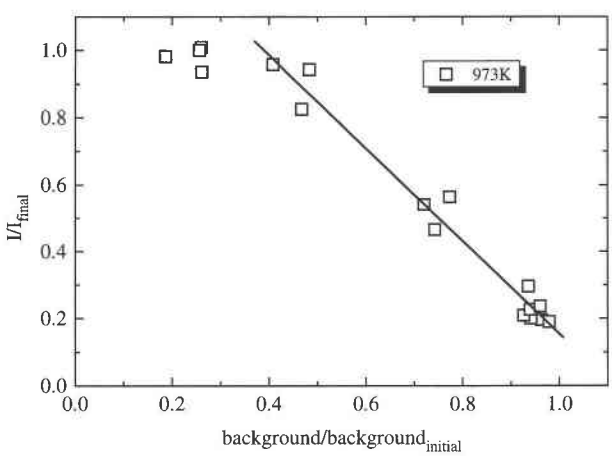

FIGURE 10. Correlation between Bragg intensity of the $(\bar{2}11)$ reflection and decrease of background scattering at 973 K.

metamict structure itself (Diaz de la Rubia 1996). A more intriguing explanation for these nuclei of undamaged structure, however, has been put forward by Holland and Gottfried (1955), who linked the appearance of these nuclei to the mechanism of metamictization itself. The observation of an equivalent secondary phase in moderately damaged titanite corroborates their model of the metamictization process.

Acknowledgments

Financial support through European Union TMR network ERB-FMRX-CT97-0108. Reviews from R.C. Ewing and G.R. Lumpkin led to substantial improvement of the manuscript.

References cited

Bismayer, U., Schmahl, W., Schmidt, C., and Groat, L.A. (1992) Linear birefringence and X-ray diffraction studies of the structural phase transition in titanite, $CaTiSiO_5$. Physics and Chemistry of Minerals, 19, 260–266.

Chrosch, J., Bismayer, U., and Salje, E.K.H. (1997) Anti-phase boundaries and phase transitions in titanite: An X-ray diffraction study. American Mineralogist, *82*, 677–681.

Diaz de la Rubia, T. (1996) Irradiation-induced defect production in elemental metals and semiconductors: a review of recent molecular dynamics studies. Annual Review of Materials Science, 26, 613–649.

Ewing, R.C. (1987) The structure of the metamict state. In Second International Conference on Natural Glasses, Prague, p. 41–48.

Ewing, R.C., Chakoumakos, B.C., Lumpkin, G.R., and Murakami, T. (1987) The metamict state. Materials Research Society Bulletin, 12, 58–66.

Finger, L.W., Cox, D.E., and Jephcoat, A.P. (1994) A correction for powder diffraction peak asymmetry due to axial divergence. Journal of Applied Crystallography, 27, 892–900.

Fleet, M.E. and Henderson, G.S. (1985) Radiation damage in natural titanite by crystal structure analysis. Materials Research Society Symposium Proceedings, 50, 363–370.

Hawthorne, F.C., Groat, L.A., Raudsepp, M., Ball, N.A., Kimata, M., Spike, F.D., Gaba, R., Halden, N.M., Lumpkin, G.R., Ewing, R.C., Greegor, R.B., Lytle, F.W., Ercit, T.S., Rossman, G.R., Wicks, F.J., Ramik, R.A., Sherriff, B.L., Fleet, M.E., and McCammon, C. (1991) Alpha-decay damage in titanite. American Mineralogist, 76, 370–396.

Hayward, P.J. (1988) Glass ceramics. In W. Lutze and R. Ewing, Eds., Radioactive waste forms for the future, p.427–492. Elsevier, New York.

Hayward, P.J. and Cecchetto, E.V. (1981) Development of sphene-based glass ceramics tailored for Canadian waste disposal conditions. In S. Topp, Ed., Scientific basis for nuclear waste management, p. 91–98. Elsevier, New York.

Higgins, J.B. and Ribbe, P.H. (1976) The crystal chemistry and space groups of natural and synthetic titanites. American Mineralogist, 61, 878–888.

Holland, H.D. and Gottfried, D. (1955) The effect of nuclear radiation on the structure of zircon. Acta Crystallographica, 8, 291–300.

Hughes, J.M., Bloodaxe, E.S., Hanchar, J.M., and Foord, E.E. (1997) Incorporation of rare earth elements in titanite: Stabilization of *A2/a* dimorph by creation of antiphase boundaries. American Mineralogist, 82, 512–516.

Larson, A.C. and Von Dreele, R.B. (1994) General structure analysis system (GSAS). Technical Report LAUR B6–748, Los Alamos National Laboratory Report, Los Alamos, New Mexico.

Lumpkin, G.R., Eby, R.K., and Ewing, R.C. (1991) Alpha recoil damage in titanite ($CaTiSiO_5$): Direct observation and annealing study using high resolution transmission electron microscopy. Journal of Materials Research, 6, 560–564.

Murakami, T., Chakoumakos, B.C., Ewing, R.C., Lumpkin, G.R., and Weber, W.J. (1991) Alpha-decay event damage in zircon. American Mineralogist, 76, 1510–1532.

Oberti, R., Smith, D.C., Rossi, G., and Caucia, F. (1991) The crystal chemistry of high-aluminum titanites. European Journal of Mineralogy, 3, 777–792.

Salje, E.K.H., Schmidt, C., and Bismayer, U. (1993a) Structural phase transition in titanite, $CaTiSiO_5$: A ramanspectroscopic study. Physics and Chemistry of Minerals, 19, 502–506.

Salje, E.K.H., Graeme-Barber, A., Carpenter, M.A., and Bismayer, U. (1993b) Lattice parameters, spontaneous strain and phase transitions in $Pb_3(PO_4)_2$. Acta Crystallographica, B49, 387–392.

Speer, J.A. and Gibbs, G.V. (1976) The crystal structure of synthetic titanite, $CaTiOSiO_4$, and the domain textures of natural titanites. American Mineralogist, 61, 238–247.

Taylor, M. and Brown, G.E. (1976) High-temperature structural study of the $P2_1/a \leftrightarrow A2/a$ phase transition in synthetic titanite, $CaTiSiO_5$. American Mineralogist, 61, 435–447.

Vance, E.R. and Metson, J.B. (1985) Radiation damage in natural titanites. Physics and Chemistry of Minerals, 12, 255–260.

Weber, W. (1990) Radiation induced defects and amorphization in zircon. Journal of Materials Research, 5, 2687–2697.

Zhang, M., Salje, E.K.H., Bismayer, U., Unruh, H.G., Wruck, B., and Schmidt, C. (1995) Phase transition(s) in titanite $CaTiSiO_5$: An infrared spectroscopic, dielectric response and heat capacity study. Physics and Chemistry of Minerals, 22, 41–49.

Zhang, M., Salje, E.K.H., and Bismayer, U. (1997) Structural phase transition near 825 K in titanite: Evidence from infrared spectroscopic observations. American Mineralogist, 82, 30–35.

Manuscript received August 26, 1997
Manuscript accepted March 30, 1998
Paper handled by George A. Lager